Exploring the $^{18}F(p,\gamma)^{19}Ne$ gateway to the formation of heavy elements in hot stars

K. E. Rehm,[1] C. L. Jiang,[1] M. Paul,[2] D. Blumenthal,[1] L. A. Daniel,[3] C. N. Davids,[1] P. Decrock,[1] S. M. Fischer,[1] D. Henderson,[1] C. Lister,[1] J. Nickles,[3] J. Nolen,[1] R. C. Pardo,[1] J. P. Schiffer,[1] D. Seweryniak,[1] and R. E. Segel[4]

[1]*Argonne National Laboratory, Argonne, Illinois 60439*

[2]*Hebrew University, Jerusalem, Israel 91904*

[3]*University of Wisconsin, Madison, Wisconsin 53706*

[4]*Northwestern University, Evanston, Illinois 60208*

(Received 29 July 1996)

An upper limit to the production of ^{19}Ne through the $^{18}F(p,\gamma)$ reaction at the recently discovered s-wave resonance has been determined. The limit implies that in a hot stellar environment ($T_9>0.5$) this reaction is not a significant gateway from the hot CNO cycle towards the production of heavier elements in stars. [S0556-2813(97)50902-2]

PACS number(s): 26.30.+k, 25.40.Lw, 25.60.−t, 27.20.+n

The isotope $^{18}F(T_{1/2}=110$ min) plays an important role in our understanding of explosive nucleosynthesis. ^{18}F is produced in the hot CNO cycle [1] and is the stepping stone to the formation of ^{19}Ne which in turn is the gateway to the rp process [2] wherein a series of (p,γ) reactions nuclei up to ^{56}Ni and beyond are produced. In a hot stellar environment ^{19}Ne can be generated either via the $^{18}F(p,\gamma)^{19}Ne$ reaction or through radiative capture of ^4He on ^{15}O with ^{15}O produced via the $^{18}F(p,\alpha)$ reaction. These reactions occur at various sites in the universe, including novae, type II supernova explosions, and x-ray bursts [1]. The $^{18}F(p,\alpha)$ and $^{18}F(p,\gamma)$ reactions are also important for controlling the production of the rare oxygen isotope ^{18}O [3]. The positive Q value for the (p,α) reaction on ^{18}F is the reason that no OF cycle exists in nature, since it allows a breakout from the cyclic reaction path $^{16}O(p,\gamma)^{17}F(\beta^+)^{17}O(p,\gamma)^{18}F(p,\gamma)^{19}Ne(\beta^+)^{19}F(p,\alpha)^{16}O$ towards ^{15}O before the final $^{19}F(p,\alpha)^{16}O$ reaction is reached.

Estimates of the astrophysical reaction rates for the $^{18}F(p,\alpha)^{15}O$ and $^{18}F(p,\gamma)^{19}Ne$ reactions have been published over the last 30 years. [4–6]. The spin values for the levels used in these calculations were taken mainly from the mirror nucleus ^{19}F. No s-wave resonance was included since no $l_p=0$ state in ^{19}Ne (or in the ^{19}F analog) was expected at the relevant excitation energy of ~7 MeV. It was therefore a surprise when in two recent experiments [7,8] evidence was found for a $3/2^+$ ($l_p=0$) state in ^{19}Ne which dominates the astrophysical reaction rate in $^{18}F(p,\alpha)^{15}O$ at temperatures $T_9>0.5$ [9]. Such an s-wave resonance could also play an important role in producing ^{19}Ne through proton capture and for this reason we have carried out the first investigation of the $p(^{18}F,^{19}Ne)\gamma$ reaction.

The experiment was performed at the ATLAS accelerator system of Argonne National Laboratory using a two-accelerator method for generating the radioactive ^{18}F ion beam [10,11]. The ^{18}F material was produced at the cyclotron of the University of Wisconsin via the $^{18}O(p,n)^{18}F$ reaction, flown to Argonne National Laboratory, and installed in the negative ion source of the ATLAS tandem injector.

Because of the relatively small cross sections (typically of the order of tens of μb) and the low γ-detection efficiency (<1%), measurements of (p,γ) cross sections usually require high beam intensities. In order to compensate for the low intensities available with today's radioactive ion beams, new techniques with considerably higher detection efficiencies are needed. An additional difficulty in experiments with radioactive ^{18}F beams is the presence of a strong contaminant from the isobar ^{18}O that required especially sensitive identification techniques in the (p,α) studies [11].

To improve the detection efficiency for radiative capture reactions, we used the fragment mass analyzer (FMA) [12] installed at the ATLAS accelerator. The FMA consists of one magnetic and two electric dipoles which disperse the particles according to p/q and E/q, respectively. Since the electric rigidity of the (p,γ) reaction products is lower than that of the beam particles by about 5%, the primary beam is stopped at a collimator located after the first electric dipole. The subsequent magnetic and electric dipoles provide for additional suppression of scattered beam particles and for the transport of the reaction products to the focal plane of the FMA where the ions are dispersed by m/q and detected in a position-sensitive parallel-grid avalanche counter. This detector is followed by a large-volume ionization chamber for Z identification. With this arrangement, a suppression factor for the incident beam relative to the (p,γ) reaction products of 10^{12} is achieved. Details of the experimental techniques will be published in a forthcoming paper [13]; a similar arrangement, involving a Wien filter combined with an additional magnetic dipole [14], has been used previously for measurements with stable beams.

The efficiency of the FMA and its detector system for radiative capture reactions was determined by measuring an excitation function for the $p(^{18}O,^{19}F)\gamma$ reaction around the previously known $l=0$ resonance in ^{19}F at $E_{c.m.}=799$ keV [15]. Beams of <0.5 particle mA of 13–17 MeV ^{18}O from the tandem accelerator were used on 80–100 $\mu g/cm^2$ CH_2 targets. In order to minimize beam induced losses of the hydrogen in the target material, a target wobbler was used that distributed the 3 mm beam spot over a ~1 cm diameter ring. The hydrogen content of the target was monitored by measuring the recoil proton yield in the course of the experiment in two monitor detectors mounted at scattering angles of ±30°.

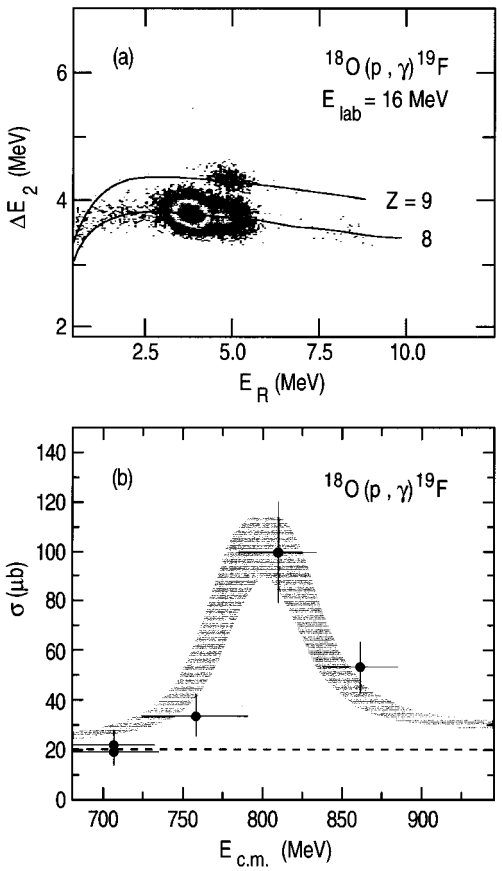

FIG. 1. (a) ΔE-E_{res} spectrum measured in the focal plane of the FMA for the $^{18}F(p,\gamma)^{19}F$ reaction. The solid lines are the result of simulations of ΔE vs E_{res} for different ions. (b) Excitation function for the $^{18}O(p,\gamma)^{19}F$ reaction. The hatched area is calculated with parameters from Ref. [16] including a 20 μb background (dashed line) caused by a small fluorine impurity in the CH_2 target.

Figure 1(a) shows a ΔE-E_{res} spectrum measured for this calibration run in the ionization chamber at an ^{18}O energy of 16 MeV. The field settings of the FMA were chosen to detect the $^{19}F^{7+}$ reaction products originating from the $^{18}O(p,\gamma)$ reaction. The ^{18}O particles originate from scattering of the incident beam at various places inside the FMA. The solid lines are the results of a simulation of ^{19}F and ^{18}O particles traversing the ionization chamber. They are in excellent agreement with the measured data.

Figure 1(b) shows the measured cross sections (solid points) as a function of the center-of-mass energy. The overall efficiency for detecting the ^{19}F particles is $30\pm3\%$. The fraction of the ^{19}F ions in the 7^+ charge state ($f_q=55\%$) was determined by measuring a charge state distribution of ^{19}F at the resonance energy. This value is in good agreement with the predictions of the charge state fractions given in Ref. [16]. The remaining part of the overall efficiency is due to the acceptance limitations imposed by a 1.7 cm wide collimater that was installed after the first electric dipole and to small angle scattering of the particles in the focal plane detector.

A comparison of this excitation function with the results obtained previously [17] shows good agreement. The hatched area in Fig. 1(b) was obtained by averaging a Breit-Wigner resonance with parameters from Ref. [17] over the target thickness of 55 keV. The yield off resonance ($\sim$20 μb) for this measurement in the FMA is dominated by recoil ^{19}F ions from a small fluorine impurity in the target and is shown as a dashed line in Fig. 1(b). This is a general problem for radiative capture measurements in inverse kinematics, when the reaction product is stable and may be present as a trace impurity in either the beam or the target. Since ^{19}Ne has a half-life of only 17.2 s, this is not a problem for the $^{18}F(p,\gamma)^{19}Ne$ experiment.

The runs with ^{18}F beams were performed at a bombarding energy (at the middle of the target) of $E_{c.m.}=670$ keV, i.e., slightly above the s-wave resonance found in the $^{18}F(p,\alpha)^{15}O$ reaction. With our target thickness of 70 keV, most of the $3/2^+$ resonance at $E_{c.m.}=652$ keV is therefore included. The integrated ^{18}F charge was determined by collecting elastically scattered ^{18}F particles on a circular aperture in the angular range $\Theta_{lab}=3.6$–$10°$ and measuring the β^+ activity on the aperture off-line after each run. The time profile of the ^{18}F exposure during the measurement and the cumulative ^{18}F activity was also monitored continuously by measuring the annihilation radiation from the collimator after the first electric dipole, where the primary ^{18}F beam was intercepted. The ^{18}F beam intensity on the CH_2 target at the fragment mass analyzer averaged over all samples was 3×10^5 ^{18}F/s with an $^{18}O/^{18}F$ ratio of about 2500:1.

Five runs with different samples of ^{18}F, each about 300 mCi, were accumulated. The data from these runs were summed and the corresponding ΔE-E_{res} spectrum is shown in Fig. 2(a). The solid lines are again simulations of the response of the ionization chamber for O, F, and Ne ions, respectively. The region where events from the $^{18}F(p,\gamma)^{19}Ne^{7+}$ reaction are expected is marked in the figure. The shape and size of this region was determined from the $^{18}O(p,\gamma)^{19}F$ measurement [see Fig. 1(a)] where it contained more than 95% of the total ^{19}F yield. There are three events that fall within this region, all of which are located close to the borderline between the $Z=9$ and 10 events. These three events have been further analyzed using the additional energy loss signal ΔE_1 from the focal plane detector. Figure 2(b) shows pulse height spectra for these three events (labeled ''^{19}Ne'') and for ^{19}F and ^{18}O particles, respectively. As can be seen from Fig. 2(b), the three events have energy loss values very close to the ones observed for ^{19}F ions. Approximating the pulse height distributions by Gaussians, one can estimate that the probability that three ^{19}Ne ions giving pulse heights as small or smaller than the observed values is less than 0.003 and we conclude that probably all three of these events are ^{19}Fe ions. The cross section corresponding to a single ^{19}Ne event is calculated to be 42 μb using the integrated charge of the ^{18}F beam (2.8 particle nC), the charge state fraction for $^{19}Ne^{7+}$ as taken from Ref. [16] and the detection efficiency which is based on the measurement of the $^{18}O(p,\gamma)$ reaction. Taking 42 μb and the widths Γ_p and Γ_t for the $3/2^+$ resonance as given in Ref. [9], a limit for the resonance strength $\omega\gamma\leqslant740$ meV and the gamma width $\Gamma_\gamma\leqslant3$ eV can be calculated. This upper limit for Γ_γ is comparable to the width obtained for the s-wave resonance populated in the $^{13}N(p\gamma)^{14}O$ reaction [18], but not as low as the limit obtained recently for a resonance in $^{19}Ne+p$ [19] where considerably higher beam cur-

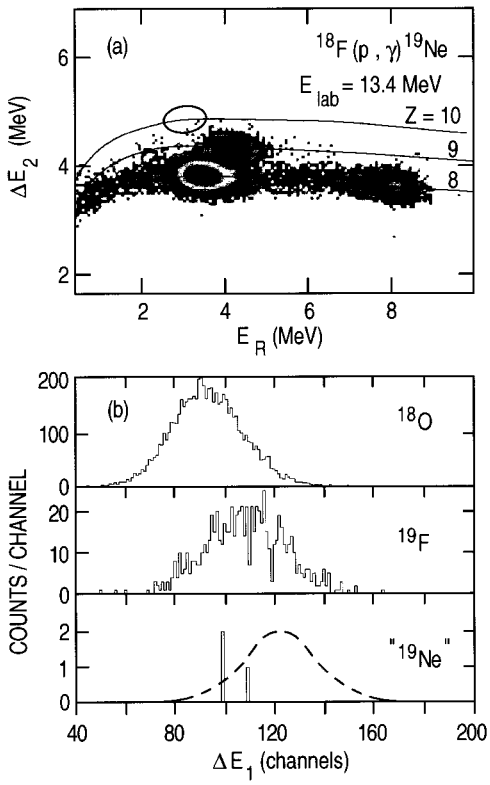

FIG. 2. (a) Same as Fig. 1(a) but measured with a ^{18}F beam containing a considerable ^{18}O contamination. The area where ^{19}Ne events from the $^{18}\mathrm{F}(p,\gamma)^{19}\mathrm{Ne}$ reaction are expected is encircled. (b) ΔE signals measured in the focal plane counter of the FMA for the three events inside the ^{19}Ne region in comparison with measured ^{19}Ne and ^{18}O events. The dashed line is the expected ^{19}Ne distribution extrapolated from the ^{18}O and ^{19}F data.

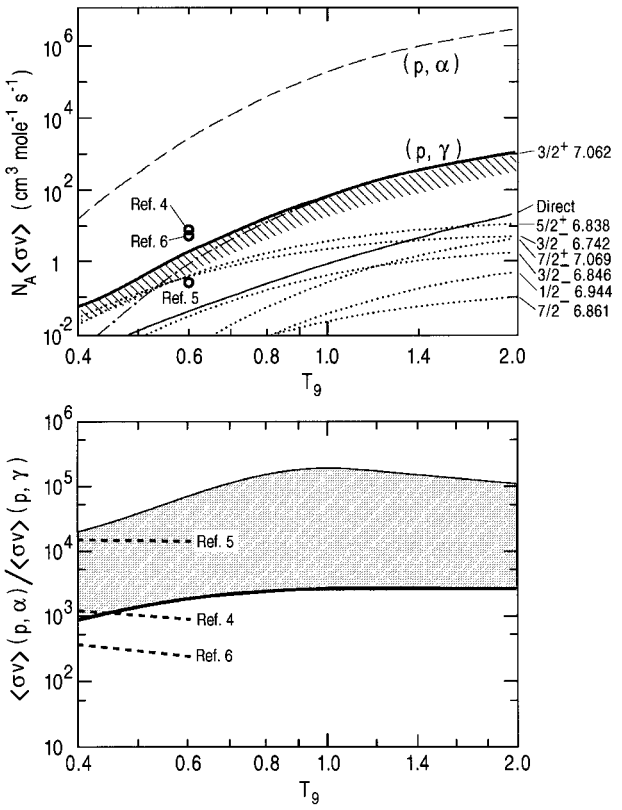

FIG. 3. (a) Limits to the astrophysical reaction rate calculated from the resonance strength determined in this experiment (thick solid line). The dashed line is the reaction rate measured for the $^{18}\mathrm{F}(p,\alpha)^{15}\mathrm{O}$ reaction in Ref. [9]. The thin solid line represents a lower limit for the reaction rate given by the direct capture process. (b) Upper and lower limits for the ratio of the reaction rates between the $^{18}\mathrm{F}(p,\alpha)^{15}\mathrm{O}$ and the $^{18}\mathrm{F}(p,\gamma)^{19}\mathrm{Ne}$ reactions. Also shown (dashed lines) are the results from previous estimates.

rents were available. A gamma width $\Gamma_\gamma = 3$ eV for the $3/2^+$ state in ^{19}Ne would correspond to about 2% of the single particle width for an $E1$ and 40% for an $M1$ transition. Transitions with such strengths have been observed in this mass region [15].

Such a limit for the radiative strength of the $3/2^+$ resonance allows one to reach some conclusions about the production of ^{19}Ne in the hot CNO cycle. The upper limit of the astrophysical reaction rate for the $^{18}\mathrm{F}(p,\gamma)^{19}\mathrm{Ne}$ reaction populating the $3/2^+$ state in ^{19}Ne as function of T_9 is shown as the dash-dot line in Fig. 3(a). Also included (dashed line) is the rate for the $^{18}\mathrm{F}(p,\alpha)^{15}\mathrm{O}$ reaction which is larger than the corresponding (p,γ) rate by at least a factor of 10^3. The estimated upper limits for other states located in this excitation energy region are shown as dotted lines in Fig. 3(a). These estimates were reached assuming the same gamma widths $\Gamma_\gamma = 3$ eV and the Γ_p/Γ values as tabulated in Ref. [9]. The upper limit for the total $p,\gamma)$ reaction rate is indicated by the thick solid line. A rough estimate for a lower limit for the (p,γ) reaction rate may be provided from a calculation of direct proton capture [17] which is shown as a thin solid line in Fig. 3(a). The symbols in Fig. 3(a) at $T_9 = 0.6$ are calculated (p,γ) reaction rates taken from the literature [4–6] none of which included the new $3/2^+$ resonance in ^{19}Ne. While consistent with the results from Ref. [5], our upper limit for the reaction rate is smaller than the values from Refs. [4,6] by factors of about three to four.

The controlling factor for the breakout from the hot CNO cycle to the rp-process is the ratio of the reaction rates $R[^{18}\mathrm{F}(p,\alpha)]/R[^{18}\mathrm{F}(p,\gamma)]$. The region allowed for this ratio by the present measurement and the direct capture calculation from Ref. [17] is given by the two solid lines in Fig. 3(b). Due to the large value of the $^{18}\mathrm{F}(p,\alpha)^{15}\mathrm{O}$ reaction rate which above $T_9 > 0.5$ is dominated by the recently discovered $3/2^+$ resonance, and a lack of a strong enhancement of proton capture from this resonance, the ratio of the reaction rates is larger than $\sim$1000 in this temperature range. This would imply that at these temperatures, the production of ^{19}Ne through the $^{18}\mathrm{F}(p,\gamma)$ reaction is probably negligible and the mechanism for generating this isotope is most likely the $^{15}\mathrm{O}(\alpha,\gamma)$ reaction, involving the more abundant ^{15}O material, although so far no direct measurements of this reaction have been performed. Also shown by the dashed lines are the results of calculated ratios from Refs. [4–6].

For proton capture on ^{18}F to be a significant competitor to the (p,α) path in this environment (similar to the case of ^{18}O) the ratio $R[^{18}\mathrm{F}(p,\alpha)]/R[^{18}F(p,\gamma)]$ would have to be $\sim$100. To achieve this, some of the lower resonances [shown as dotted lines in Fig. 3(a)] would need a considerably larger ratio for $\Gamma_\gamma/\Gamma_\alpha$. Since the alpha particle decay widths Γ_α for these resonances are known from the mirror nucleus ^{19}F, unprecedented large values for Γ_γ ($\sim$30 eV, or 20% of

a Weisskopf unit) would be needed for at least one of these resonances.

The present work provides the first direct experimental limit for the ratio of the reaction rates between the $^{18}F(p,\alpha)^{15}O$ and the $^{18}F(p,\gamma)^{19}Ne$ reactions. The large cross section for the first reaction makes the (p,γ) route a small branch for the production of ^{19}Ne at temperatures $T_9 > 0.5$, where this nuclide is produced more effectively via the $^{15}O(\alpha,\gamma)$ reaction.

The use of the fragment mass analyzer for the measurement of radiative capture reactions in inverse kinematics results is a considerable improvement over gamma detection techniques, especially when the reaction products are unstable. Improvements in beam intensity, which should be possible for less chemically reactive elements, should allow the use of thinner targets and thus the measurement of excitation functions in finer steps.

The authors want to thank J. Truran (University of Chicago) for valuable discussions and J. Greene for his help with the target production and the thickness measurements. This work was supported by the U.S. Department of Energy, Nuclear Physics Division under Contract No. W-31-109-ENG-38, the National Science Foundation, and by a University of Chicago/Argonne National Laboratory Collaborative Grant.

[1] A.E. Champagne and M. Wiescher, Annu. Rev. Nucl. Part. Sci. **42**, 39 (1992).
[2] R.K. Wallace and S.E. Woosley, Astrophys. J. Suppl. **45**, 389 (1981).
[3] H. Norgaard, Astrophys. J. **215**, 200 (1977).
[4] R.V. Wagoner, Astrophys. J. Suppl. **18**, 247 (1969).
[5] S.E. Woosley, W.A. Fowler, J.A. Holmes, and B.A. Zimmerman, At. Data Nucl. Data Tables **22**, 371 (1978).
[6] M. Wiescher and K.U. Kettner, Astrophys. J. **263**, 891 (1982).
[7] K.E. Rehm *et al.*, Phys. Rev. C **52**, R460 (1995).
[8] R. Coszach *et al.*, Phys. Lett. B **353**, 184 (1995).
[9] K.E. Rehm *et al.*, Phys. Rev. C **53**, 1950 (1996).
[10] A. Roberts *et al.*, Nucl. Instrum. Methods Phys. Res. B **103**, 523 (1995).
[11] K.E. Rehm *et al.*, Nucl. Instrum. Methods Phys. Res. A **370**, 438 (1996).
[12] C.N. Davids, B.B. Back, K. Bindra, D.J. Henderson, W. Kutschera, T. Lauritsen, Y. Nagame, P. Sugathan, A.V. Ramayya, and W.B. Walters, Nucl. Instrum. Methods Phys. Res. B **70**, 358 (1992).
[13] K. E. Rehm *et al.* (unpublished).
[14] M.S. Smith, C. Rolfs, and C. Barnes, Nucl. Instrum. Methods Phys. Res. A **306**, 233 (1991).
[15] F. Ajzenberg-Selove, Nucl. Phys. **A475**, 1 (1987).
[16] K. Shima, N. Kuno, M. Yamanouchi, and H. Tawara, At. Data Nucl. Data Tables **51**, 173 (1992).
[17] M. Wiescher, H.W. Becker, J. Görres, K.-U. Kettner, H.P. Trautvetter, W.E. Kieser, C. Rolfs, R.E. Azuma, K.P. Jackson, and J.W. Hammer, Nucl. Phys. **A349**, 165 (1980).
[18] P. Decrock *et al.*, Phys. Rev. Lett. **67**, 808 (1991).
[19] R.D. Page *et al.*, Phys. Rev. Lett. **73**, 3066 (1994).